Quantifying the pattern of microbial cell dispersion, density and clustering on surfaces of differing chemistries and topographies using multifractal analysis

David Wickens [a,c] Stephen Lynch[b] Glen West[c] Peter Kelly[c] Joanna Verran[a] Kathryn A. Whitehead[a,c*]

[a]School of Healthcare Science, Manchester Metropolitan University, Chester St, Manchester M1 5GD UK

[b]School of Computing, Mathematics and Digital Technology, Manchester Metropolitan University, Chester St, Manchester M1 5GD UK

[c]Surface Engineering Group, Manchester Metropolitan University, Chester St, Manchester M1 5GD UK

E-mail addresses: davidjwickens@gmail.com; s.lynch@mmu.ac.uk; g.west@mmu.ac.uk; peter.kelly@mmu.ac.uk; j.verran@mmu.ac.uk;

*Corresponding author: K.A.Whitehead@mmu.ac.uk +44 (0) 161 247 1157

Abstract

The effects of surface topography on bacterial distribution across a surface is of extreme importance when designing novel, hygienic or antimicrobial surface coatings. The majority of methods that are deployed to describe the pattern of cell dispersion, density and clustering across surfaces are currently qualitative. This paper presents a novel application of multifractal analysis to quantitatively measure these factors using medically relevant microorganisms (*Staphylococcus aureus* or *Staphylococcus epidermidis*). Surfaces (medical grade 316 stainless steel) and coatings (Ti-ZrN, Ti-ZrN/6.0%Ag, Ti-ZrN/15.6%Ag, TiZrN/24.7%Ag) were used in microbiological retention assays. Results demonstrated that *S. aureus* displayed a more heterogeneous cell dispersion ($\Delta\alpha_{AS} < 1$) whilst the dispersion of *S. epidermidis* was more symmetric and homogeneous ($\Delta\alpha_{AS} \geq 1$). Further, although the surface topography and chemistry had an effect on cell dispersion, density and clustering, the type of bonding that occurred at the surface interface was also important. Both types of cells were influenced by both surface topographical and chemical effects however, *S. aureus* was influenced marginally more by surface chemistry whilst *S. epidermidis* cells was influenced marginally more by surface topography, thus this effect was bacterially species specific. The results demonstrate that multifractal analysis is a method that can be used to quantitatively analyse the cell dispersion, density and clustering of retained microorganisms on surfaces. Using quantitative descriptors has the potential to aid the understanding the effect of surface properties on the production of hygienic and antimicrobial coatings.

Keywords

Alloys; Bacteria; Clustering; Density, Dispersion; Multifractal

1. Introduction

Bacterial attachment to, and retention on a surface is a thoroughly documented prerequisite for biofilm formation (Hamadi et al., 2014). It is recognised in the literature that biofilm formation may result in increased infection and failure rates of implants and devices, including external bone fixation devices (van der Borden et al. 2007; Hosman et al. 2009). Many engineered surfaces used in both medical and industrial situations present, either by design or due to wear, topographical surface features of different sizes and shapes that may be of regular or irregular dispersion across the surface (Flint et al. 2001; Whitehead and Verran 2006). The topography of a surface is thought to be one of the factors that contribute towards increased microbial contamination and fouling (Verran and Whitehead 2006; Rechendorff et al. 2006; Whitehead and Verran 2007; Whitehead et al. 2011). Surface topography may enhance microbial retention because of the increased surface area available for colonisation by increasing the microorganism-material interface and, in some cases, by protecting cells from shear stress (Cooper et al. 2011). Micro and nano roughness commonly occur in finishes of stainless steel surfaces used in medical equipment and also orthopaedic implants (Luong-Van et al. 13). The nano-roughness of a surface is important especially in orthopaedic applications because the nanotopography of a surface can affect the behaviour of bacterial cells and how they adhere (Colon et al., 2006; Xu and Siedlecki 2012) and also the behaviour of the bone cells and their ability to adhere to the surface during osseointegration (Anselme et al. 2010). It is suggested that the method of altering the surface roughness (at the nano scale) to prevent adhesion of bacteria without the use of drugs may be one of the best ways to reduce orthopaedic implant infection (Campoccia et al. 2006; Puckett et al. 2010).

The topography of any surface will take the form of a series of peaks and troughs which may vary in both profile, dispersion and density, described to some extent by parameters such as R_a

(Arithmetic average height), R_q (Root mean square roughness), R_t (Difference between the single largest peak and single deepest valley across the scan area) and R_z (Sum of the height of the largest profile peak height (R_p) and the largest profile valley depth (R_v) within a sampling length) (Table 1). Although methods to describe surface topography and features are commonly used, attempts to directly relate any of these parameters solely to bacterial cell retention have not always been successful (Truong et al. 2010). Though it has been suggested that surface topography can affect cell retention (Jullien et al. 2003; Whitehead et al. 2011), others have found no relationship (Medilanski et al. 2002; Hilbert et al. 2003), thus it may be suggested that appropriate quantitative descriptors are somewhat lacking (Mabboux et al. 2004; Zhao et al. 2008). Thus, novel methods to further describe the dispersion, density and clustering of cells across a surface in relation to their surface properties are needed.

Multifractal analysis may be one approach to gain numerical data on the effect of surface topography on cell dispersion, density and clustering. A fractal is an object that displays self-similarity under magnification and can be constructed using a simple motif (an image repeated on ever-reduced scales). A multifractal is a generalization of a fractal, where a single dimension is not enough to describe it. Instead, a continuous spectrum of dimensions is required. Although fractals are idealized images that cannot exist in nature, multifractal objects abound in the realms of science. There has been an ongoing surge of interest in multifractal analysis for describing both artificial and physical objects and concepts have been increasingly applied across a wide range of scientific disciplines. Biologically related subjects include human heartbeat dynamics (Ivanov et al. 1999), ageing and disease relations in physiology (Goldberger 2002), and the detection of breast cancer (Li et al. 2007). In terms of microbiological applications, Kropp et al. (1997) carried out a restricted multifractal analysis of microbially induced magnesium calcite formation in recent tidal

sediments using binary elemental dot maps. Thus the abundance of multifractal analysis use in research shows that the potential for use in microbiological applications is viable. Thus, the aim of this work was to determine if multifractal analysis could be used to quantify cell dispersion, density and clutering and relate these values to trends demonstrated in the surface properties (chemistry and topography).

2. Material and Methods

2.1 Production and analysis of surfaces and coatings

Medical grade 316L stainless steel (Aalco, UK) was cut into 10 x 10 x 1.5 mm coupons. The side to be coated had been prepared by the manufacturer to a fine polish surface finish (R_a < 10 nm). Prior to coating, the surfaces were cleaned with isopropanol and methanol (Sigma, UK) by wiping the surfaces with a fibre free cloth (Buhler, USA). Any remaining physical contaminants were removed by a blast of dry nitrogen gas and the samples were placed in the vacuum chamber to be immediately coated. The magnetron sputter deposition for this investigation was undertaken using a Teer Coatings Ltd. UDP 350 sputtering system in a closed field, unbalanced magnetic configuration. Power was supplied to the magnetron using a Pinnacle Plus (Advanced Energy, USA) mid-frequency pulsed-dc power supply. A -30 V bias was applied to the substrate holder using an MDX DC power supply (Advanced Energy, USA). The metallic interlayers were deposited as follows; the sputtering system contained three targets: titanium, zirconium and silver (300 x 100 mm, 99.95% purity). The substrates were sputter cleaned at 150W, 100kHz and 90% duty for 20 minutes in 0.4 Pa argon. A titanium layer was deposited at 100 kHz and 90% duty at 1 kW for four minutes with the substrate holder rotating at 16 RPM. Following deposition of the titanium interlayer, a pure zirconium interlayer was deposited for three minutes at 1.5 kW, 300 kHz, 50% duty, until the reactive sputter controller (controlled feedback via plasma optical

emissions monitoring - OEM) was turned on at 80% of the full metal signal (FMS) of zirconium. The reactive gas (nitrogen) flow was graded by varying the OEM setting from 80% down to 45% FMS decreasing the set point in 5% increments every 30 seconds. Once the zirconium was being sputtered in full reactive mode (45% FMS) power was applied to the silver target of 90 W, 130 W and 160 W for coatings containing 5 at.%, 15 at.% and 24.6 at.% silver respectively. Pulse frequency of 300 kHz and 50 % duty were used throughout the ZrN/Ag co-sputtering process. The entire coating run, excluding the 4 minutes of titanium deposition, totalled one hour to achieve a 1 μm thickness and was left for 45 minutes to cool following deposition to reduce stress induced by mismatches in thermal expansion for the film layers and substrate. Atomic force microscopy (Quesant, UK) was performed on the surfaces to obtain topography values. The AFM was operated using silicon nitride tips with a force constant of 0.12 N m^{-1} in contact mode, at a speed of 2Hz.

2.2 Microbiology and retention assays

The microorganisms *Staphylococcus aureus* NCTC 8532 and *Staphylococcus epidermidis* NCTC 11057 were used for this investigation. Stock cultures were stored in the freezer at -80 ºC. When required, the cultures were thawed and inoculated onto Brain Heart Infusion (BHI) agar (Oxoid, UK) and incubated for 24 h at 37 ºC. The inoculated agar plates were kept refrigerated at 4 ºC and replaced every four weeks. Sterile BHI broth (Oxoid, UK) (10 ml) was inoculated with *S. aureus* NCTC 8532 or *S. epidermidis* NCTC 11057. These were incubated overnight in an orbital incubator at 37 ºC for 24 hours at 130 RPM. Cultures were removed from incubation and the cells were washed once by centrifuging at 604 *g* for 10 minutes. The supernatant was removed and the cells were re-suspended in sterile distilled water. Cells were diluted to an optical density (OD) of 1.0 ± 0.05 at 540 nm using a spectrophotometer (Jenway 6305, UK), using distilled water as a blank. Cell numbers were determined in colony forming units ml^{-1} (CFU ml^{-1}) using serial dilutions

down to 1 x 10^{-8}. The diluted cell suspension (100µl) was spread and repeated in duplicates on BHI agar and incubated at 37 ºC for 24 h. For the retention assays, three replicate substrata were placed horizontally in a glass Petri dish, to which 30 ml of a standardised cell suspension was added, and incubated at 37 ˚C for 1 hour without agitation. Following incubation, the test pieces were removed and rinsed once, gently with 5 cm^3 distilled H_2O, with the distilled water bottle at a 45˚ angle, with a 3 mm nozzle. The samples plus retained bacteria were air dried onto substrata in a laminar flow hood for 1 h. Assays were repeated in duplicate (Whitehead and Verran 2007). Retained cells were stained using 0.03% acridine orange dissolved in 2% glacial acetic acid (Sigma, UK) for 10 minutes. Following staining, the cell-substrate samples were rinsed in sterile deionised membrane filtered water, and air dried in a class 2 laminar flow hood. The substrata plus adherent microorganisms were visualised using epifluorescence microscopy (Nikon Eclipse E600, UK) at 400× magnification and 10 sample fields were captured for analysis from each substratum using Cell-F (Olympus, UK). The epifluorescence images were used in the MATLAB®, Image Processing Toolbox® for the multifractal analysis. Statistical tests were carried out using one way ANOVA and student t-tests. The results were reported as mean ± standard error. The differences observed between the substrates were considered significant at $p < 0.05$.

2.3 Examples of multifractal $f(\alpha)$ spectra and multifractal analysis box counting

To illustrate the properties of typical multifractal spectra, multifractal datasets were computed for each motif using MATLAB®. Using a simple iterative program, matrix (datasets) of size 512 × 512 were computed by overlaying the given motifs one on top of another, so that upon the first iteration a 4×4 matrix was formed, upon the second iteration a 8×8 matrix was formed, until completion. Using the MathWorks Image Processing Toolbox, the datasets were converted into grayscale images; a value of zero would give black on this scale and a value of one would give

white. The numerical $f(\alpha)$ spectra were computed for, $-10 \le q \le 10$, and boxes of size ε = 4, 8, 16, 32, 64, 128 and 256, were used to fully cover the datasets. From the $f(\alpha)$ curves there are values that can be read which denote numerical values of the bacterial density, clustering and dispersion. D_0, the maximum value of the $f(\alpha)$ curve (when $q = 0$), gives a numerical value for the density of the cells on the surface (Fig. 1) whilst $\Delta\alpha = \alpha_{max} - \alpha_{min}$, describes the heterogeneity of the cell spread on the surface. Alongside the $f(\alpha)$ curves, analysis of the images was undertaken to also determine the maximum area of a single point/cell on an image (Max-A) the total coverage of the cells across the whole image as a percentage (% coverage). A measure of clustering can also be achieved by looking at the symmetry of the $f(\alpha)$ curve.

In multifractal analysis, typically, experimental data and model simulations can give highly non-uniform probability distributions possessing scaling behaviour and self-similarity. The method adopted was based on the $f(\alpha)$ singularity spectrum which is computed using the methods outlined in Chhabra et al. (1989). Multifractal analysis was applied to provide statistical properties for the objects in terms of their generalized (box-counting) fractal dimensions (Hentschel and Procaccia 1983) or their singularity spectrum (Halsey et al. 1986).

The generalized (box-counting) fractal dimensions D_q, where $q \in \Re$, (where q is a real number) are defined by;

$$D_q = \lim_{\varepsilon \to 0} \frac{1}{1-q} \frac{\ln \sum_{i=1}^{N} p_i^q(\varepsilon)}{-\ln \varepsilon} \quad , \qquad (1)$$

where the index i labels the individual boxes of size ε and $p_i(\varepsilon)$ denotes the relative weight of the i'th box or the probability of the object lying in the box. The probability $p_s(\varepsilon)$ of segments of type s scales with the size ε of a box and is calculated as follows:

$$p_s(\varepsilon) \propto (\varepsilon)^{\alpha_s} \ , \tag{2}$$

where α_s is the so-called coarse Hölder exponent defined by:

$$\alpha_s = \frac{\ln p_s(\varepsilon)}{\ln \varepsilon} . \tag{3}$$

The number of segments N_s of type *s* scales with the size ε of a box are calculated according to**:**

$$N_s(\varepsilon) \propto (\varepsilon)^{-f_s} . \tag{4}$$

The exponents α_s and f_s are then used to determine the $f(\alpha)$ spectrum. In many cases, $f(\alpha)$ is related to the Hausdorff-Besicovich dimension (Falconer 2103; 2014).

The image to be analysed was covered with boxes of size ε and the corresponding box-measures $\mu_i(\varepsilon) = p_i(\varepsilon)$ were computed. The Hausdorff dimension of the measure-theoretic support of $\mu(q)$ is given by;

$$f(q) = \lim_{\varepsilon \to 0} \frac{\sum_{i=1}^{N} \mu_i(q,\varepsilon) \ln \mu_i(q,\varepsilon)}{\ln \varepsilon} \tag{5}$$

and

$$\alpha(q) = \lim_{\varepsilon \to 0} \frac{\sum_{i=1}^{N} \mu_i(q,\varepsilon) \ln p_i(\varepsilon)}{\ln \varepsilon} \ , \tag{6}$$

where $\mu_i(q,\varepsilon)$ are the normalized probabilities

$$\mu_i(q,\varepsilon) = \frac{p_i^q(\varepsilon)}{\sum_{j=1}^{N} p_j^q(\varepsilon)} \ . \tag{6}$$

The epifluorescent images of the cells on the surfaces were analysed in two ways. In the first case, gray-scale images were used to measure dispersion. In the second case, the images were converted to black (surface) and white (cells) binary files using the MathWorks Image Processing Toolbox; where black pixels were assigned values of zero and white pixels one. Multifractal analysis was carried out on both sets of images and the computed curves plotted. Ten images of each of the surfaces with retained microorganisms were processed and the averages calculated.

Following acquisition of the $f(\alpha)$ spectra, the quantitative outputs were calculated. The minimum value of α was denoted by "α_{min}", ($q = +\infty$). The "α_{max}", was the point at which the curve intersected with the *x*-axis at $q = -\infty$. The "α_0" depicts the value at which the maximum of $f(\alpha)$ exists. Using the data cursor in MATLAB®, the two points α_{max} and α_{min} were estimated and used to give a measure of the dispersion ($\Delta\infty$) as follows:

$$\Delta\infty = \alpha_{max} - \alpha_{min}$$

and a measurement of asymmetry ($\Delta\alpha_{AS}$) as given by

$$\Delta\alpha_{AS} = \frac{(\alpha_0 - \alpha_{min})}{(\alpha_{max} - \alpha_0)}.$$

The $\Delta\alpha_{AS}$ values corresponds to whether the $f(\alpha)$ curve was skewed left or right, the curve is

- symmetric if $\Delta\alpha_{AS} = 1$;
- left skewed if $\Delta\alpha_{AS} > 1$;
- right skewed if $\Delta\alpha_{AS} < 1$.

3. Results and Discussion

Multifractal analysis was used to quantitatively determine the dispersion, density and cell clustering values of bacteria retained on a range of antimicrobial surfaces. The $f(\alpha)$ singularity spectrum used in this work provided a more intuitive description of the multifractal measure than the complicated geometrical interpretation of the D_q values. Both methods are equivalent and

transforms exists that convert one spectrum to another (Lynch 2007) (2010) (2014). It is essential that the boxes cover the whole image and no pixels are missed, otherwise the multifractal analysis will not work, therefore images need to be cropped to the required 512×512 pixels if they are of another dimension. In order to demonstrate how different data affects the $f(\alpha)$ spectra examples of modal data were produced. These examples include data for a motif with one value smaller than the other three quarters (Fig. 2a); in terms of cell distribution, this would denote a left skew, due to the majority of the image being densely packed with cells but still with areas of space. When one value was greater than the other three quarters (Fig. 2b) this results in a right skew that would indicate the cells being sparsely distributed but with somewhat of a small, densely grouped area on the images. If there are roughly equal values for all four quarters (Fig. 2c), this results in a symmetrical curve which denotes a sparsely distributed cell pattern with little to no grouping or very few, widely, regularly spaced cells on the surface (a narrow spectrum indicates homogeneity). Thus it can be demonstrated how the $f(\alpha)$ curves (Fig. 3) are affected by the values chosen in the motifs displayed (Fig. 2).

The theoretical (solid curves) and corresponding numerically computed ('+') multifractal $f(\alpha)$ spectra are displayed (Fig. 3a-c) for the motifs shown (Fig. 2a-c). The $f(\alpha)$ curve gives a measure of cell distribution. It was demonstrated that the line $f(\alpha)=\alpha$ was tangent to the $f(\alpha)$ spectrum at the point $q=1$. The points where the $f(\alpha)$ curve met the α axis were labelled $\alpha_{\max}$ and $\alpha_{\min}$, where $\alpha_{\max} > \alpha_{\min}$. The maximal value of the $f(\alpha)$ curve gives the fractal dimension of the object, denoted by D_0 and was equal to $f(\alpha)$ when $q=0$ (Lynch, 2010).

By converting an image to a black and white image, a measure of density may be calculated using multifractal theory. An example of a black and white version of an image is shown (Fig. 4) and

the corresponding $f(\alpha)$ curve computed for $-1 \le q \le 1$ is shown (Fig. 5a). A zoom in to the region where the maximal value occurs and the data cursor can be used to approximate this value is also demonstrated (Fig. 5b). The maximum value of the *f*(α) curve gives the fractal dimension D_0, which gave a statistical measure of how the object fills the space.

Using the first method on the original images, the fractal dimension (or density) D_0 was equal to two for all of the multifractal objects since the objects cover the whole plane. The widths ($\Delta\infty = \alpha_{\max} - \alpha_{\min}$ values) of the $f(\alpha)$ spectra indicated the heterogeneity or dispersion of the multifractal object. If the widths of the spectra are widespread, this illustrates that these multifractal objects were more heterogeneous (Fig. 3a -b). In fact, the multifractal generated by the motif (Fig. 2a) was the most heterogeneous, with a $\Delta\infty = \alpha_{\max} - \alpha_{\min}$ value of approximately 5.5. The $\Delta\infty = \alpha_{\max} - \alpha_{\min}$ value (Fig. 3b) was approximately 3 and the $\Delta\infty = \alpha_{\max} - \alpha_{\min}$ value (Fig. 3c) was approximately 0.5. In most physical applications a problem arises with negative values of q (values from the left side of the *f*(α) curve); boxes where low measurement may contribute disproportionately. Several papers have been published addressing this so-called clipping problem (Pastén et al. 2011; Veneziano 2009) but they are beyond the scope of this paper.

One hypothesis of this work was to determine if there was a relationship between the quantitative cell dispersion, density and clustering values derived using MATLAB® which could be related to the surface chemistry or topography values. The addition of the coating did not increase the underlying surface values, as can be determined by comparing the stainless steel and Ti-ZrN coatings. However, an increase in silver concentration led to an increase in surface nanotopograhy, demonstrated by the increase in roughness values (Fig. 5). Following SEM backscattered electron detection it was determined that the increase in surface roughness was due to outlying particles of

embedded silver protruding from the surface (data not shown). The R_a value is generally used as a parameter for comparison of surface roughness (Hilbert et al. 2003; Whitehead and Verran 2006). An R_a value of less than 800 nm has been ascribed to a hygienic stainless steel surface (Flint et al. 1997). The R_a values for the surfaces analysed in this work were significantly below the threshold value for a hygienic surface (range 4.3 ± 0.8 to 8.3 ± 1.4 nm). The R_a, R_q and R_t values increased with increasing silver concentration. The average height (R_z) values demonstrated a different trend, whereby an increase was observed with increasing silver concentration of the surfaces, with the exception of the Ti-ZrN.15.6% Ag surface which demonstrated the greatest value, possible due to larger protruding silver particles from the surface. The reason for this phenomenon at this level of silver concentration will be investigated in future work.

The application of multifractal analysis was used to examine the dispersion, density and clustering of the microorganisms by using a monochrome image (Fig 6). The images were taken using epifluorescent microscopy to demonstrate the pattern of retention of *S. aureus* and *S. epidermidis* microorganisms on the test surfaces and then the images converted to monochrome for multifractal analysis. Multifractal analysis was used to determine a qualitative value of the dispersion of the bacteria on the surfaces (Fig 7). The results demonstrated that for *S. aureus* dispersion of the cells across all the surfaces was heterogeneous. The least heterogeneous spread was observed on the Ti-ZrN/24.7at.% Ag surfaces. In contrast, *S. epidermidis* displayed a more symmetric or homogeneous dispersion. Only the Ti-ZrN and the Ti-ZrN/24.7at.%Ag displayed heterogeneous *S. epidermidis* cell dispersion across the surfaces. The Ti-ZrN/6.0at.% Ag and Ti-ZrN/15.6at.% Ag surfaces demonstrated the most homogeneous cell dispersions.

In terms of cell dispersion, density and clustering on the surfaces, patterns emerged that could be related to the chemical and topographical properties of the surfaces. If the surfaces are considered

as two chemically different substrata, for example if the stainless steel and Ti-ZrN are grouped as ceramics and the Ti-ZrN Ag containing surfaces are metallic then some interesting trends arose. This can be reasoned due to differences in the chemical bonding in the surfaces since stainless steel has a chromium oxide layer, whilst Ti-ZrN is a ceramic, thus the two surfaces may act in a similar manner. The silver was dispersed in the coatings as nano-particles and thus may have metallic components at the surface-cell interface; these differences in the two groups of coatings may go some way to explain the microbial:MATLAB® results observed. Thus for the dispersion results, *S. aureus* cells increased between the stainless steel and ZrN surfaces, whilst the number of *S. epidermidis* cells decreased and no trend of *S. aureus* cell number could be related to the increased surface roughness of the silver surfaces, thus demonstrating a chemical effect of the surfaces on cell dispersion. However, there was an influence of both topography and chemistry demonstrated on the pattern of *S. epidermidis* cell dispersion on the silver surfaces whereby there was a decrease in the number of cells with an increase in roughness values.

For the density results (Fig. 8), the microorganisms showed different behaviour on the ceramic surfaces; the density of *S. aureus* decreased with increasing *R* values whilst *S. epidermidis* increased with increasing *R* values. On the silver containing surfaces, *S. aureus* numbers followed the average height (R_z) values whereas *S. epidermidis* numbers decreased with increasing *R* values. Thus, it may be determined that both surface topography and chemistry had an effect on *S. aureus* density on the ceramic surfaces, whilst surface topography affected *S. aureus* density on the silver surfaces. Surface chemistry and topography both had an effect on the density of *S. epidermidis* on both the silver and ceramic surfaces and these effects were cell species specific.

For the cell clustering results (Fig. 9) *S. aureus* demonstrated an increase in the clustering on the Ti-ZrN when compared to the stainless steel surface which was indicative of a chemical effect of

the surface. However, on the metallic surfaces, cell clustering then decreased in value on the Ti-ZrN/6.0at.% Ag surface and then increased with increasing amounts of silver in the coatings, in line with the *R* values which was indicative of a topographical effect. For the *S. epidermidis* cells, the opposite trend was seen for the stainless steel and the Ti-ZrN surface in that clustering decreased from the stainless steel surface when compared to the Ti-ZrN. For the silver containing surfaces, *S. epidermidis* clustering followed the average height (R_z) trends, thus it may be speculated that a chemical effect was demonstrated to affect the clustering on the cells on the ceramic surfaces and topographical effects determined the cell clustering patterns on the silver surfaces.

If the results were collated together (Fig. 10), a pattern emerged in that, it was demonstrated that the ceramic surfaces tended to chemically influence the patterns of the cells on the surfaces, whilst the silver surfaces demonstrated a greater topographical effect. Thus, it may be considered that once a nano- topography occurs, this demonstrated an influence on the pattern of cell retention. Further, both types of cells were influenced by both surface topographical and chemical effects however, *S. aureus* was influenced marginally more by surface chemistry whilst *S. epidermidis* cells were influenced marginally more by surface topography.

A crucial step in multifractal analysis is in determining the range of box sizes ($l \le \varepsilon \le L$) and the range of order *q* over which the analysis is to be applied. One possible solution was suggested by Aharony (1990). In the mathematical equations (7) and (8) below there are limits as the box sizes $\varepsilon \to 0$, which are not physically realizable, but In practice, one constructs lines of best fit using linear regression for

$$\sum_{i=1}^{N} \mu_i(q,\varepsilon) \ln \mu_i(q,\varepsilon) \text{ versus } \ln \varepsilon \qquad (7)$$

and

$$\sum_{i=1}^{N} \mu_i(q,\varepsilon) \ln p_i(\varepsilon) \text{ versus } \ln \varepsilon . \quad (8)$$

in order to approximate $f(q)$ and $\alpha(q)$, respectively. The number and scale of box sizes is vitally important in the analysis and care needs to be taken as a consequence. Thus, in this paper, images of dimensions 512 x 512 pixels were cropped from the original images and black and white versions were constructed using image analysis techniques with the MathWorks Image Processing Toolbox. Using these dimensions, boxes from a range of sizes $\varepsilon = 4,8,16,32,64,128$ and 256 were chosen to cover the images completely. It was suggested (Posadas et al. 2003) that a correlation coefficient of $R^2 = 0.94$ or above would be sufficient in order for the multifractal analysis to work correctly. By restricting q values to $-10 \le q \le 10$, and by using a selection of the box dimensions stated above, it was ensured that the correlation coefficients remained above $R^2 = 0.98$, for all of the examples considered in this paper.

Stainless steel samples with already defined and characterised surface features were used for the underlying substrate for the sputter coating. This was to reflect an applied application of coating a commercial external bone fixation pin. There has been some debate, as to whether surface topography is important in cell retention, however, if it is, it would seem likely that it might be a factor involved in maintaining the hygienic status of a surface, or in the prevention of cross contamination. Thus, advances that allow quantification of cellular dispersion, density and clustering across substrata are invaluable to the understanding of such cell-surface interface interactions. The use of multifractal analysis provided insightful analysis in that it demonstrated that it was not only the surface topography and chemistry that had an effect on cell dispersion, density and clustering but also the type of bonding that occurred at the surface interface was important. The results taken from the multifractal analysis proved to be successful in quantitatively

describing all three descriptors of the retained bacterial cells on the different surfaces. Thus, this work demonstrates a novel application of multifractal analysis to measure these parameters of bacterial cell density and dispersion on various surfaces.

4. Conclusions

The aim of the investigation was to utilise MATLAB® to demonstrate if retained microorganism on a range of surfaces could be quantified in terms of dispersion, density and clustering. The results demonstrated that MATLAB® was an extremely successful tool to quantify these factors. Results demonstrated that although the surface topography and chemistry had an effect on cell dispersion, density and clustering, the type of bonding that occurred at the surface interface was also important. It was demonstrated that the ceramic surfaces tended to chemically influence the patterns of the cells on the surfaces, whilst the silver surfaces demonstrated a greater topographical effect therefore once a nano-topography occurs, this demonstrated an influence on the pattern of cell retention. Both types of cells were influenced by both surface topographical and chemical effects however, *S. aureus* was influenced marginally more by surface chemistry whilst *S. epidermidis* cells were influenced marginally more by surface topography. Giving quantitative descriptors to describe the retained bacteria on surfaces has the potential to aid the production of hygienic surfaces that may be used in a range of medical and other industries.

References

Anonymous (2010) BS 1134:2010 Assessment of surface texture. Guidance and general information: British Standards Institute UK

Aharony A (1990) Multifractals in physics – successes, dangers and challenges. Physica A 168:470-489

Anselme K et al (2010) The interaction of cells and bacteria with surfaces structured at the nanometre scale. Acta Biomaterialia 6**:**3824-3846

Campoccia D et al (2006) The significance of infection related to orthopedic devices and issues of antibiotic resistance. Biomaterials 27**:**2331-2339

Chhabra et al (1989) Direct determination of the f (alpha) singularity spectrum and its application to fully-developed turbulence. Phys Rev A 40**:**5284-5294

Colon et al (2006) Increased osteoblast and decreased *Staphylococcus epidermidis* functions on nanophase ZnO and TiO2. J Biomed Mater Res A 78**:**595-604

Cooper et al. (2011) Engineered antifouling microtopographies: kinetic analysis of the attachment of zoospores of the green alga Ulva to silicone elastomers. Biofouling 27**:**881-891.

Falconer K (2103) Fractals - A Very Short Introduction. Oxford University Press.

Falconer K (2014) Fractal Geometry: mathematical Foundations and Applications. Wiley-Blackwell.

Flint et al (1997) Biofilms in dairy manufacturing plant description, current concerns and methods of control. Biofouling 11:81-97

Flint S et al (2001) The growth of *Bacillus stearothermophilus* on stainless steel. J Appl Microbiol 90:151–157

Goldberger AL (2002) Fractal dynamics in physiology: Alterations with disease and aging. PNAS 99: 2466–2472

Halsey TC et al (1986) Fractal measures and their singularities: the characterisation of strange sets. Phys Rev A 33:1141-1151

Hamadi F et al (2014) Adhesion of Staphylococcus aureus on stainless steel treated with three types of milk. Food Control 38:104-108

Hentschel HE and Procaccia I (1983) The infinite number of generalised dimensions of fractals and strange attractors. Physica D8:435–444

Hilbert LR et al (2003) Influence of surface roughness of stainless steel on microbial adhesion and corrosion resistance. Inter Biodeter Biodegrad 52:175-185

Hosman AH et al (2009) Metal-on-metal bearings in total hip arthroplasties: influence of cobalt and chromium ions on bacterial growth and biofilm formation. J Biomed Mater Res A 88:711–716

Ivanov PC et al (1999) Multifractality in human heartbeat dynamics. Nature 399:461-465

Jullien C et al (2003) Identification of surface characteristics relevant to the hygienic status of stainless steel for the food industry. J Food Eng 56**:**77-87

Kropp J et al (1997) Multifractal characterization of microbially induced magnesian calcite formation in Recent tidal flat sediments. Sedimentary Geol 109**:**37-51

Li H et al (2007) Fractal Analysis of Mammographic Parenchymal Patterns in Breast Cancer Risk Assessment. Academic Radiology 14**:**513-521

Lynch S (2007) Dynamical Systems with Applications using Mathematica®, Springer

Lynch S (2010) Dynamical Systems with Applications using Maple™ 2nd Edition, Springer

Lynch S (2014) Dynamical Systems with Applications using MATLAB® 2nd Edition, Springer

Luong-Van E et al (2013) Review: Micro- and nanostructured surface engineering for biomedical applications. 28:165-174

Mabboux F et al (2004) Surface free energy and bacterial retention to saliva-coated dental implant materials—an *in vitro* study. Colloids Surf B: Biointerfaces 39**:**199-205

Medilanski E et al (2002) Influence of the surface topography of stainless steel on bacterial adhesion. Biofouling 18:193-203

Pasten D et al (2011) Monofractal and multifractal analysis of the spatial distribution of earthquakes in the central zone of Chile. Phys Rev E 84**,** 066123

Posadas AND et al (2003) Multifractal characterization of soil pore systems. Soil Sci Soc Am J 67**:**1361-1369

Puckett SD et al (2010) The relationship between the nanostructure of titanium surfaces and bacterial attachment. Biomaterials 31**:**706-713

Rechendorff K et al (2006) Enhancement of protein adsorption induced by surface roughness. Lamgmuir 22:10885-10888

van der Borden AJ et al (2007) Prevention of pin tract infection in external stainless steel fixator frames using electric current in a goat model. Biomaterials 28:2122-2126

Veneziano D and Furcolo P (2009) Improved moment scaling estimation for multifractal signals. Nonlinear Processes Geophysics 16:641-653

Verran J and Whitehead KA (2006) Assessment of organic material and microbial components on hygienic surfaces. Food Bioproducts Processing 84:260-264

Whitehead KA and Verran J (2006) The effect of surface topography on the retention of microorganisms. Food and Bioproducts Processing 84**,**:253-259

Whitehead KA and Verran J (2007) The effect of surface properties and application method on the retention of *Pseudomonas aeruginosa* on uncoated and titanium-coated stainless steel. Inter Biodeter Biodeg 60:74-80

Whitehead KA et al (2011) The antimicrobial properties of titanium nitride/silver nanocomposite coatings. J Adh Sci Tech 25:2299-2315

Xu L-C and Siedlecki CA (2012) Submicron-textured biomaterial surface reduces staphylococcal bacterial adhesion and biofilm formation. Acta Biomaterialia 8**:**72-81

Zhao Q et al (2008) Reduction of bacterial adhesion on ion-implanted stainless steel surfaces. Med Eng Phys 30:341-349

Figure Legends

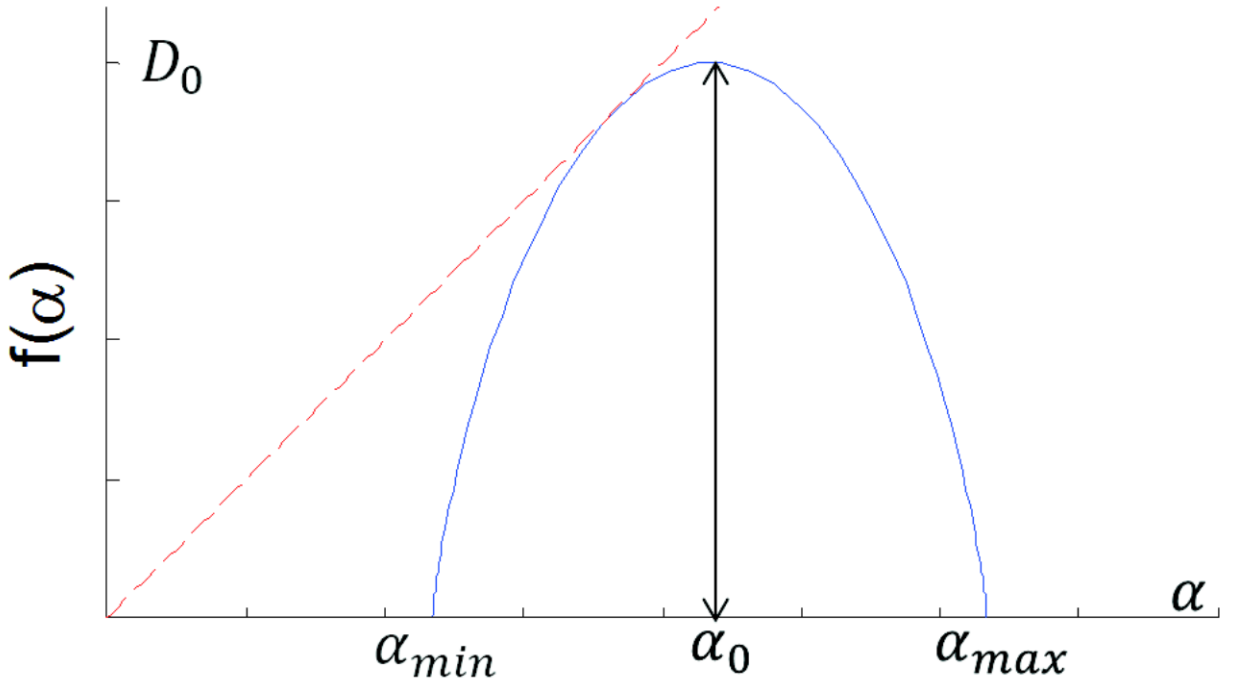

Fig. 1 A typical *f*(α) curve with denotations of the α_{min}, α_0 and α_{max}, displaying a multifractal spectrum

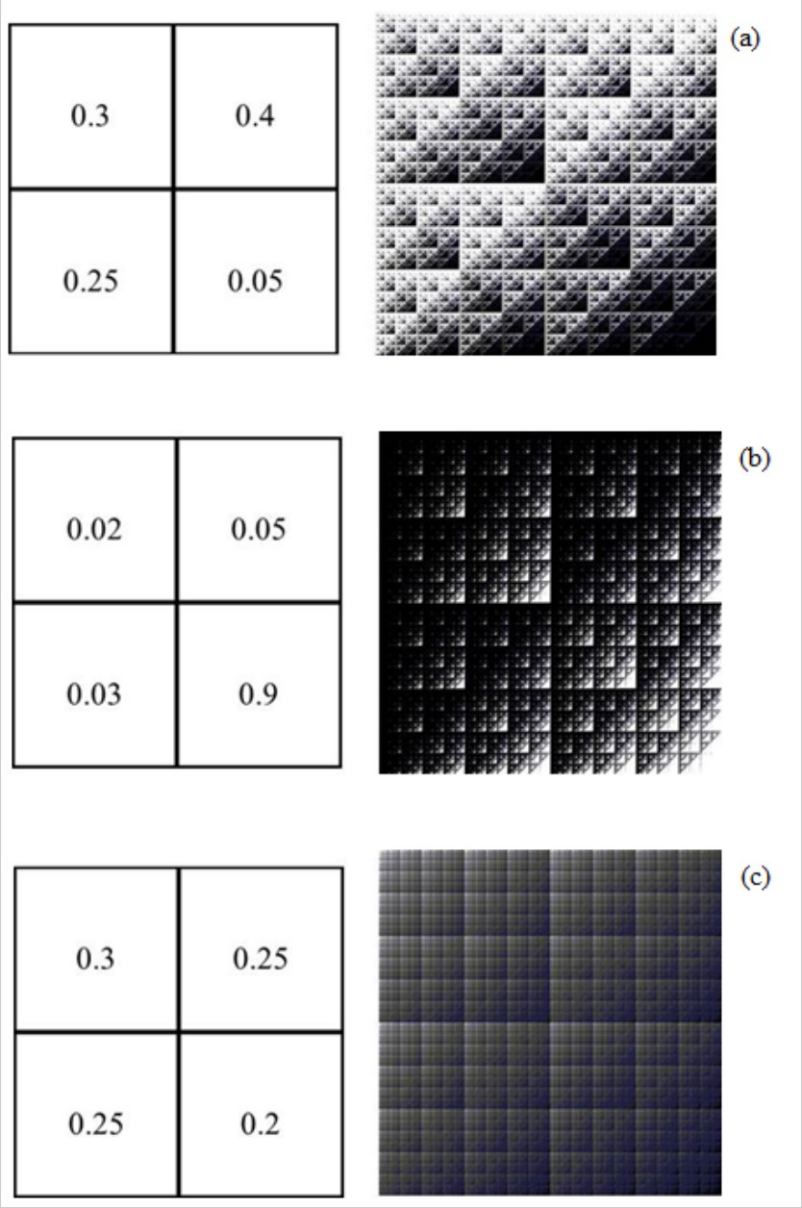

Fig. 2 Multifractal motif examples. Theoretical and numerical singularity spectra for the multifractal generated with (a) the motif with one value much smaller than the other three quarters, giving a heterogeneous arrangement. (b) the motif with one value much greater than the other three quarters, the most heterogeneous (largest $\Delta\alpha_{as}$) and (c) the motif with similar values for all four quarters, the most homogeneous result (smallest $\Delta\alpha_{as}$).

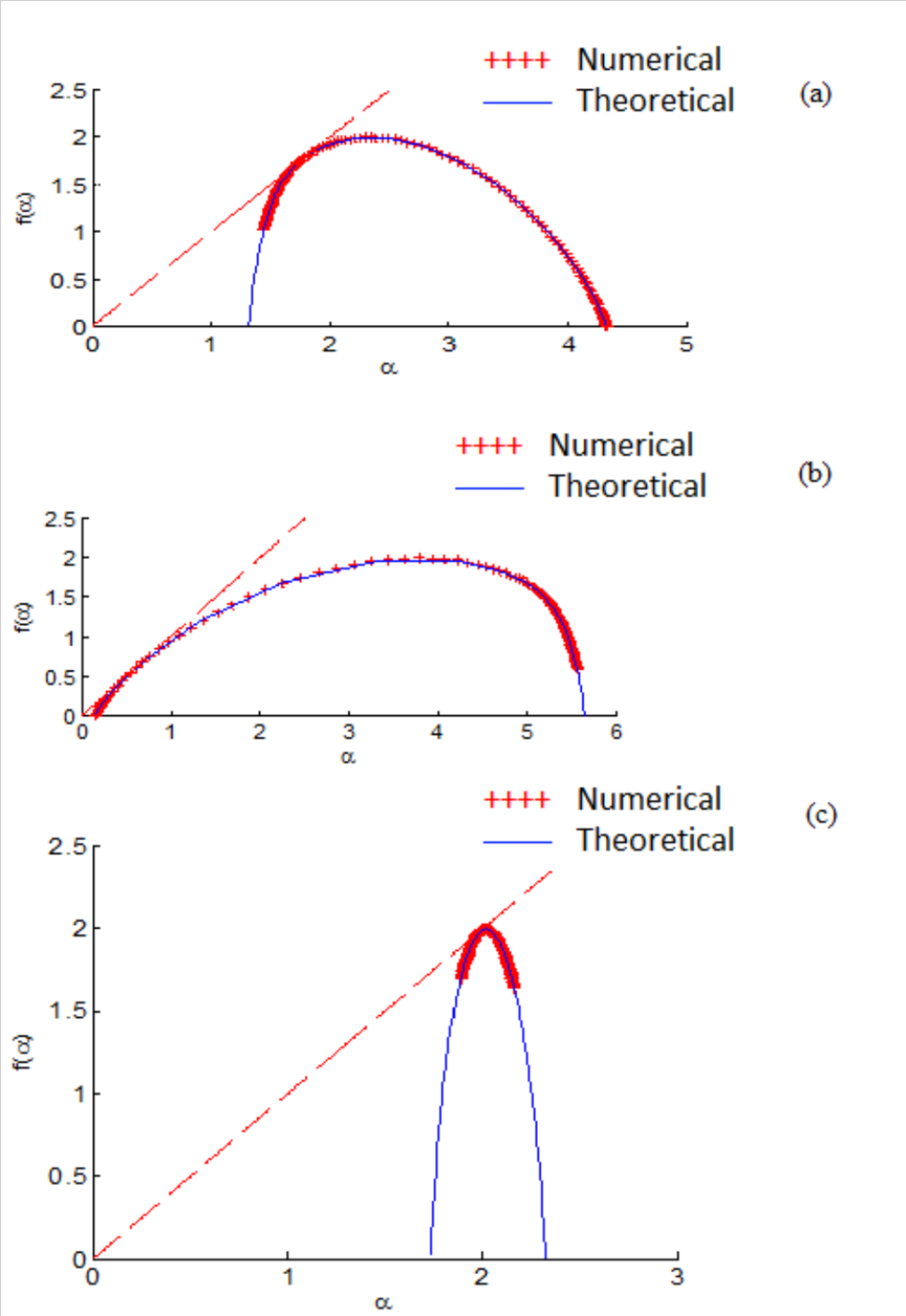

Fig. 3 The corresponding $f(\alpha)$ curves for the multifractal motifs shown in Figure 2: (a) right sided skewness, (b) left sided skewness and (c) near symmetrical/homogeneous distributions

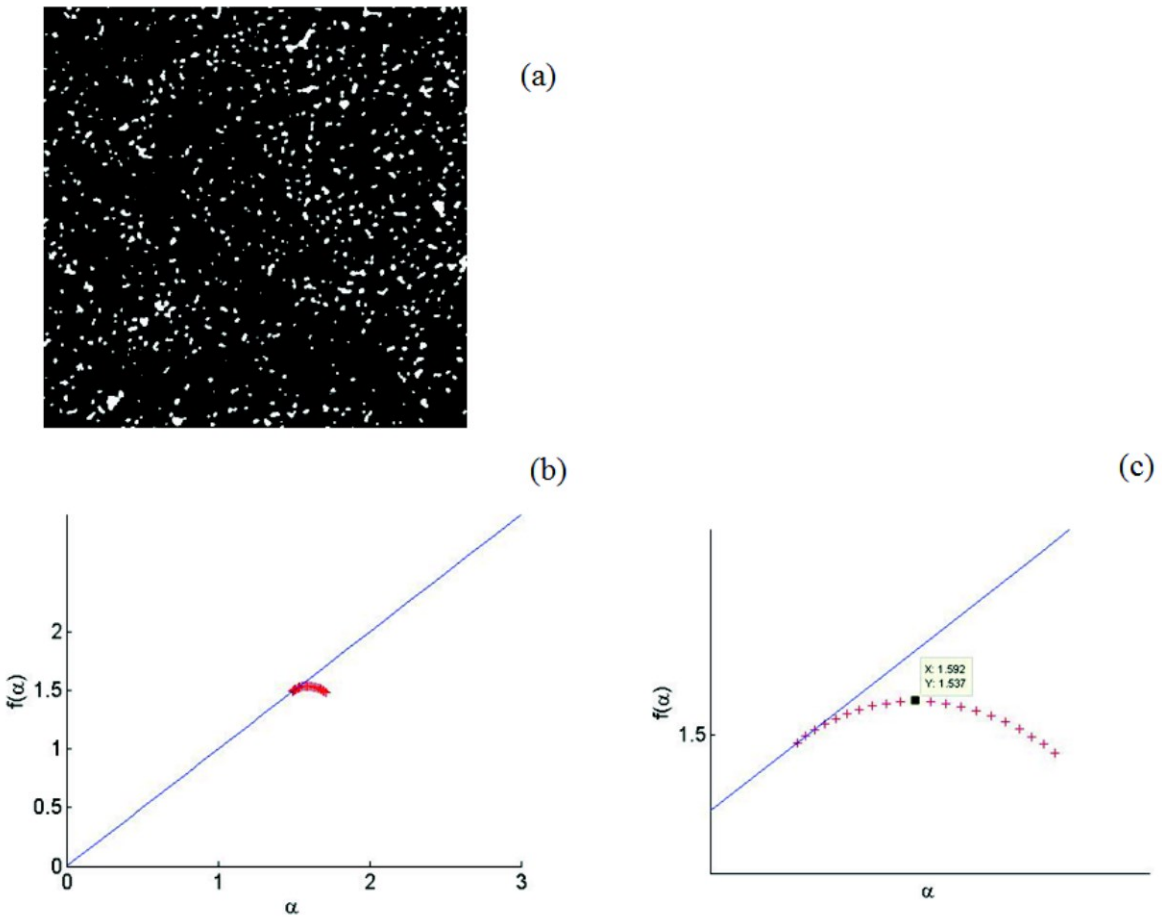

Fig. 4 (a) A black and white image of the cells on a surface (b)The $f(\alpha)$ spectrum for the image shown in Fig. 4 when $-1 \leq q \leq 1$. (c) A zoom in on the local maximum and labelling of this point using the MATLAB® data cursor

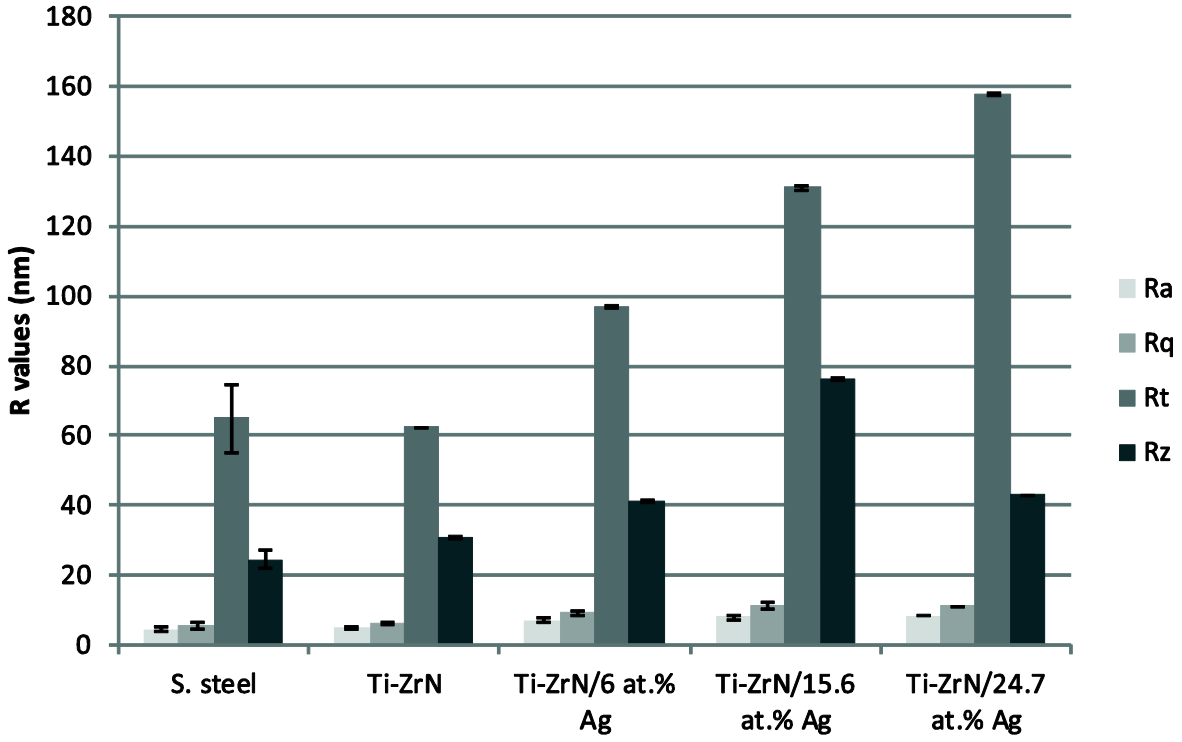

Fig. 5 *R* values quantified using AFM (10 x 10 μm) demonstrating the topography of the surfaces (n = 15)

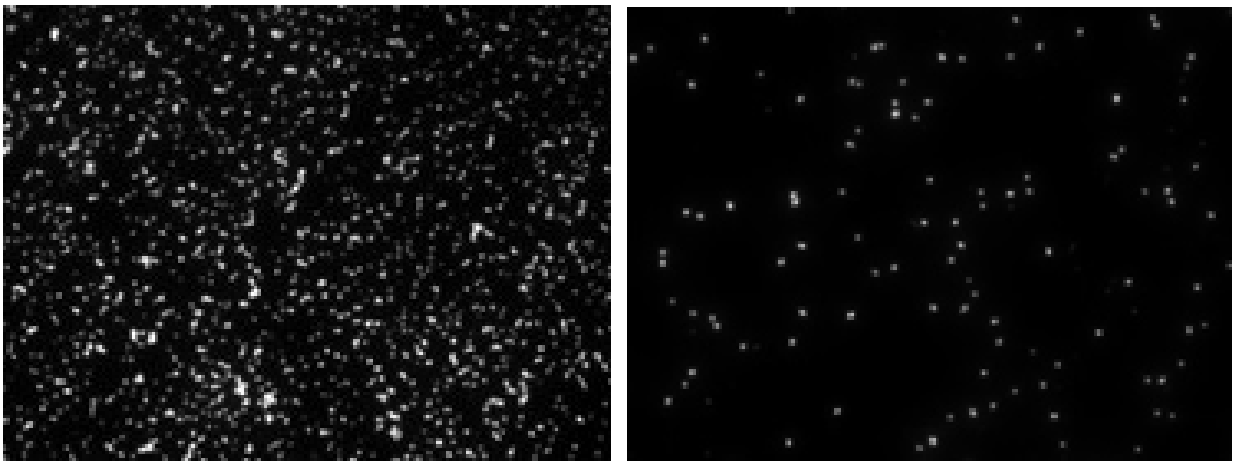

Fig. 6 The application of multifractal analysis was used to examine the dispersion, density and clustering of the microorganisms by using a monochrome image (magnification x 400)

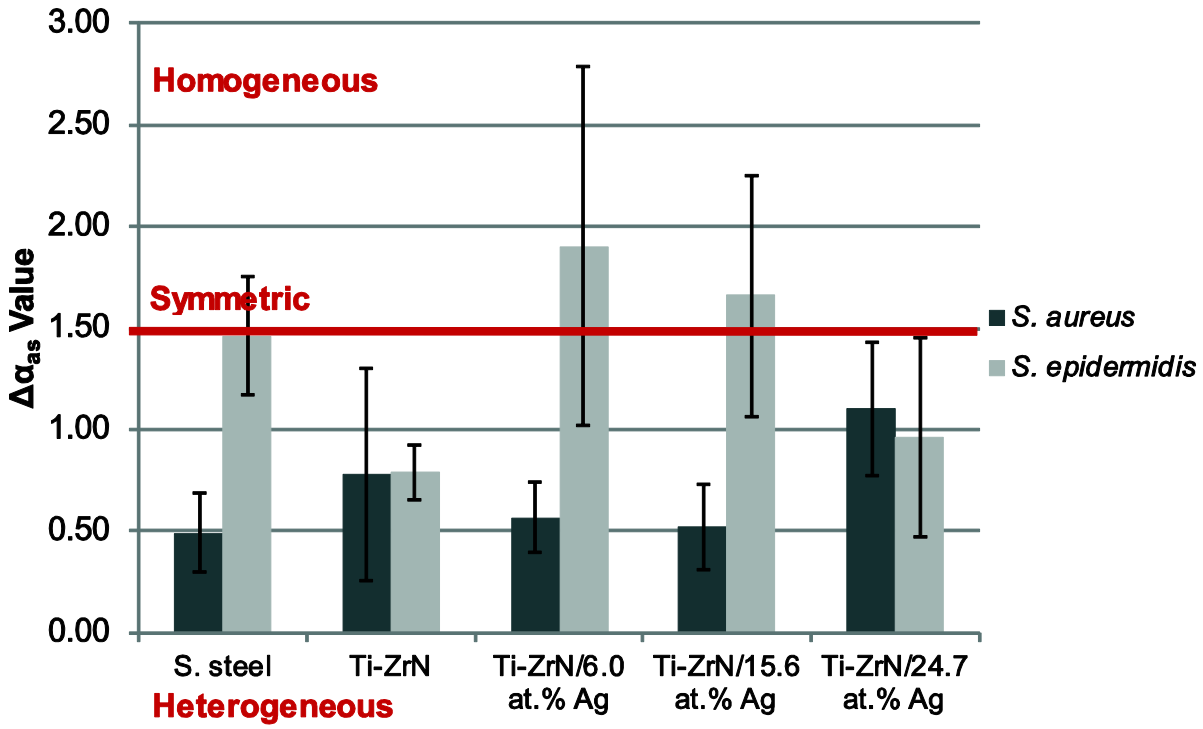

Fig. 7 Δαas values of *S. aureus* and *S. epidermidis* on the surfaces demonstrating the difference in homogeneity and heterogeneity between the two microorganisms on the different surfaces (n = 30). The *S. aureus* was primarily of heterogeneous spread with the exception of 24.7 at.% silver. The *S. epidermidis* was more homogeneous for the majority with the 6.0 at.% silver surface being the most homogeneous and became more symmetric as the silver content increased

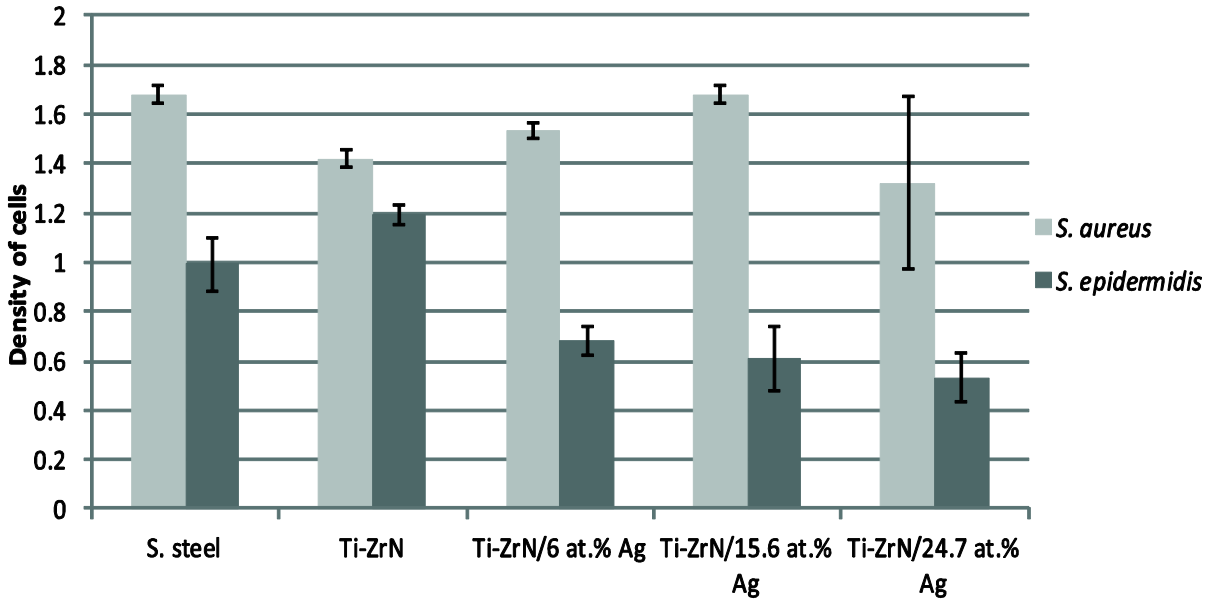

Fig. 8 Density of *S. aureus* and *S. epidermidis* demonstrating that the microorganisms showed different behaviour on the ceramic surfaces when compared to the silver containing surfaces (n = 30)

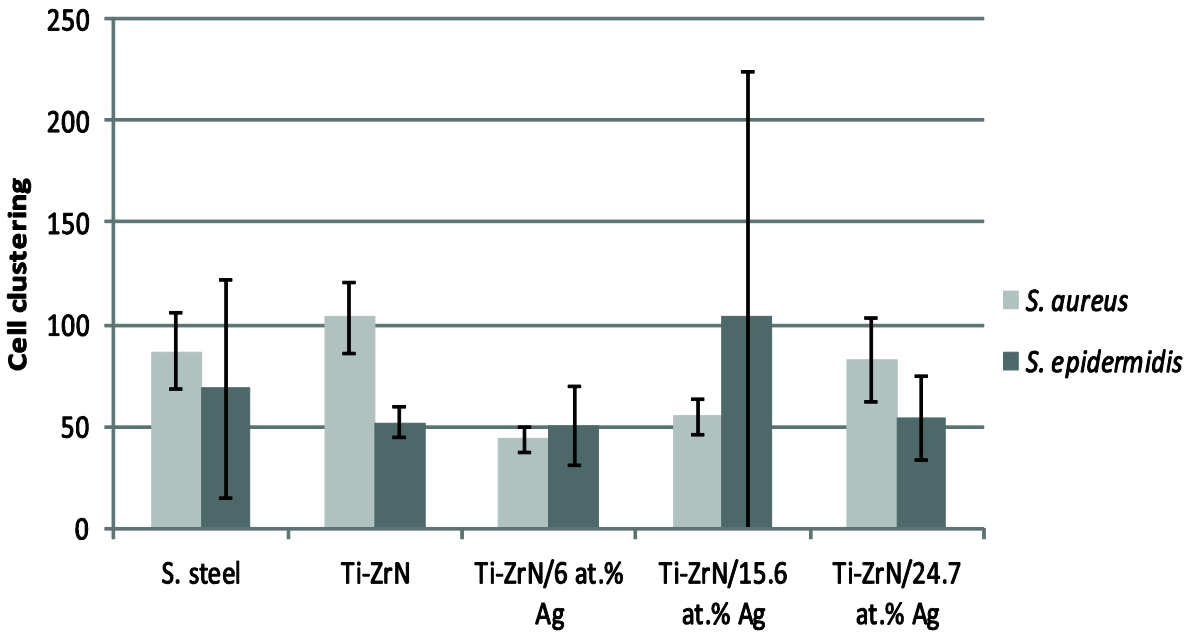

Fig. 9 Clustering of *S. aureus* and *S. epidermidis* demonstrated that both surface topography and chemistry affected cell distribution (n = 30)

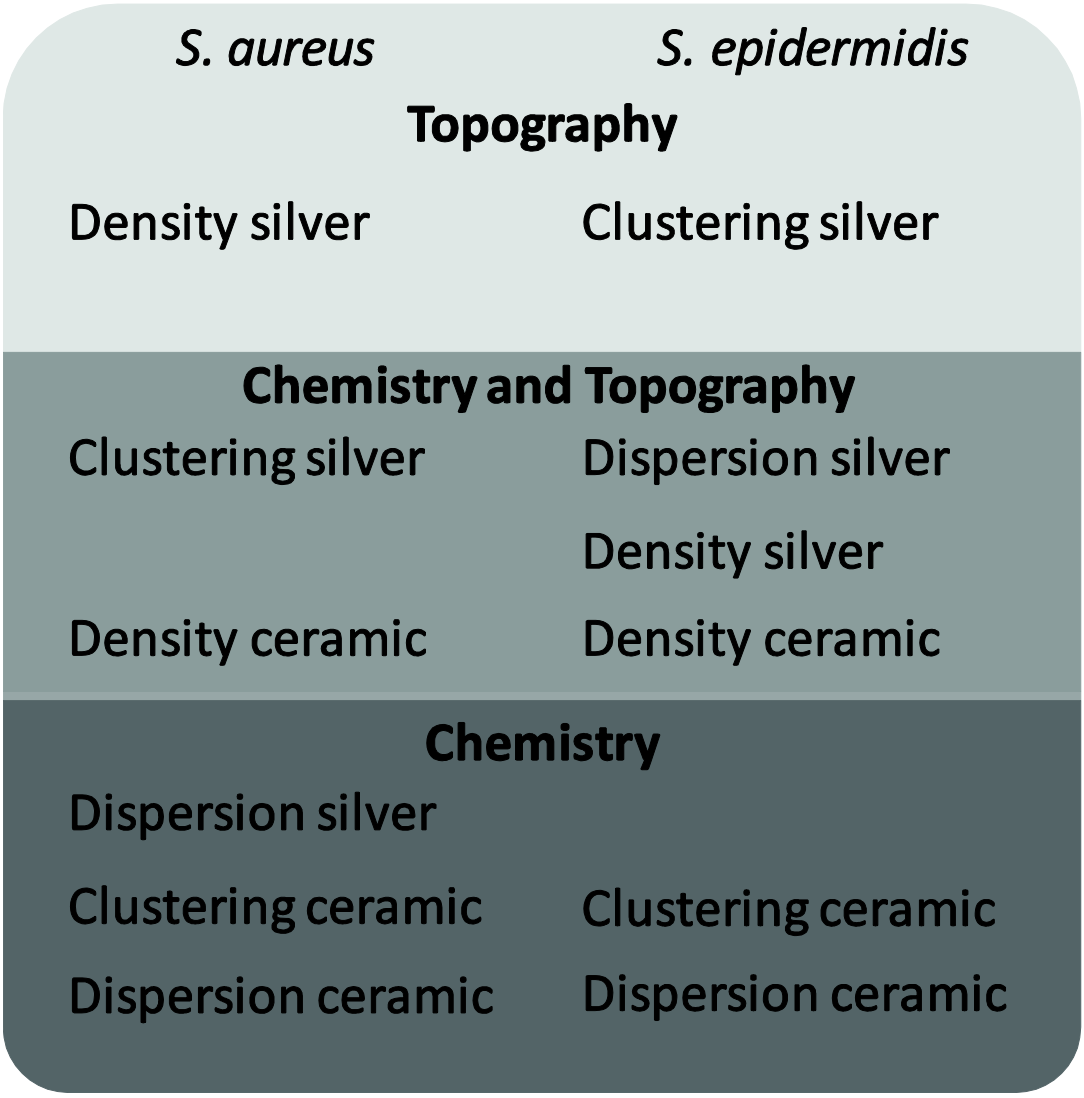

Fig. 10 Schematic diagram used to demonstrate the surface property trends (chemistry and topography) that affected cell dispersion, density and clustering. The ceramic surfaces tended to chemically influence the patterns of the cells on the surfaces, whilst the silver surfaces demonstrated a greater topographical effect. Both types of cells were influenced by both surface topographical and chemical effects however, *S. aureus* was influenced marginally more by surface chemistry whilst *S. epidermidis* cells were influenced marginally more by surface topography.

Table 1 Definitions of the surface roughness measurements used to describe the different topographical characteristics of the substrata (Anon 2010)

	Other names	Definition
R_a	Centre Line average	Arithmetic average height
R_q	(RMS)	Root mean square roughness
R_t	(Max range)	Difference between the single largest peak and the single deepest valley across the scan area
Rz	(Average Height)	The sum of the height of the largest profile peak height (R_p) and the largest profile valley depth (R_v) within a sampling length